A Reachability-Based Method for Large-Signal Behavior Verification of DC-DC Converters

Eric M. Hope, *Student Member, IEEE*, Xichen Jiang, *Student Member, IEEE*, and Alejandro D. Domínguez-García, *Member, IEEE*

***Abstract*—A method for large-signal behavior verification of power electronics DC-DC converters subject to uncertain variations in operating conditions is proposed. This method relies on the computation of the reach set, i.e., the set of all possible trajectories that arise from different initial conditions, unknown-but-bounded inputs, and inherent switching. Large-signal behavior verification is accomplished by checking that the reach set remains within the region of state-space defined by performance requirements, e.g., output voltage tolerance specifications, component voltage and current limits. Algorithms to solve the reachability problem for power electronics converters operating under both open- and closed-loop control are provided along with simulations illustrating the proposed method.**

I. Introduction

Several types of analyses are used to verify DC-DC converter behavior against design performance requirements. The purpose of these analyses is to ensure the entire system behaves as expected under all possible operating conditions. Analysis techniques include (see, e.g., [1], [2], [3], [4] and the references therein): i) open-loop, large-signal simulation, ii) small-signal average modeling for controller design, iii) closed-loop, large-signal system behavior verification, and iv) switching detail modeling. In open-loop, large-signal simulation, an ideal converter model is used to simulate the voltage and current waveforms. In small-signal average modeling, a small-signal average model is used to design a controller that ensures stability of system dynamic response to small perturbations on the source- or load-side. In large-signal system behavior verification, lengthy time-domain simulations are conducted to analyze the system response to large disturbances. In switching detail modeling, simulations are conducted to obtain over-voltages, power losses, and other component stresses due to nonlinearities in switching devices, stray inductances, or capacitances.

This paper focuses on the problem of *large-signal behavior verification*, and proposes an alternative to time-domain simulation-based methods. In this work, power electronics converters are described by a switched-linear state-space representation, where the system inputs, e.g., load current and source voltage, may vary over some bounded range. The proposed method relies on the computation of the set of possible trajectories that arise from different initial conditions, inputs, and inherent switching, which is known in literature as *reach set computation* [5]. It can be used to determine if performance requirements in the form of maximum deviations of certain system states are met under all possible operating conditions. This can be accomplished by checking whether the reach set is contained in a region of the state-space defined by performance requirements. This research has relevance in applications where tight static and transient performance requirements are required, e.g., voltage module regulators for microprocessor power supplies [6], [7], [8].

Literature is reviewed on existing methods for large-signal behavior verification of power electronics systems. Time-domain simulation-based Monte Carlo analysis has been used extensively for both verification and design of converters [8], [9], [10], [11], [12], [13]. For example, in [8], Monte Carlo analysis is used to verify the design of a specific voltage regulator module for the Intel Core i7 Processor in the presence of uncertainties in component values and operational conditions. In [9], the authors propose a verification technique for power supply systems that breaks the complex system into several models of varying complexity before applying Monte Carlo analysis to verify the system at each level. Monte Carlo analysis can also be used to search the entire parameter design space, e.g., component values, and controller gains, in order to select an optimal design in terms of minimizing cost and maximizing performance. For example, Monte Carlo has been applied to converter feedback loop compensation circuit designs in order to achieve optimal performance [11], [12], and to the selection of converter parameter values in order to mitigate electromagnetic interference [13]. A drawback of Monte Carlo analysis is the large number of time-domain simulations required to span the entire design parameter space and operational conditions. As the size and complexity of the system increase, Monte Carlo analysis becomes less tractable.

Other methods for quantifying large-signal behavior of power electronics do not rely on time-domain simulations [7], [14], [15]. For example, the work in [7] develops analytical models to bound the envelope of trajectories around an average converter trajectory. The motivation behind our work is similar, but the approach, which relies on the Krylov-Bogoliubov-Mitropolsky averaging method, is quite different to ours. In our approach, which relies on reachability analysis techniques, a large-signal switching model is used; the algorithms provided produce extremely accurate bounds on the set containing all possible values attained by state trajectories that arise from

The authors are with the Department of Electrical and Computer Engineering of the University of Illinois at Urbana-Champaign, Urbana, IL 61801, USA. E-mail: aledan@ILLINOIS.EDU.

This work was supported in part by the National Science Foundation (NSF) under grant ECCS-CAR-0954420.

switching and input variations.

The use of reachability analysis techniques in power electronics has been proposed previously for analyzing reliability of fault-tolerant power electronics systems [16], where the problem was formulated in terms of the converter linearized average model, without including the converter switching behavior. The use of large-signal switching models was proposed in [17], where input variations are contained in an ellipsoidal set. This paper substantially extends [17] by: i) providing a precise formulation of the reachability problem in DC-DC converters; ii) tailoring ellipsoidal-based reachability tools to cases when the input space is defined by a symmetric polytope; iii) providing a more detailed analysis of open- and closed-loop controlled buck and boost converters; iv) providing a detailed comparison of the computational performance of the proposed method with simulation-based Monte Carlo methods; and iv) providing a method to address parametric uncertainty.

The remainder of this paper is organized as follows. Section II introduces the power electronics converter model considered and provides the necessary background on reachability analysis of dynamical systems. Section III provides the algorithms for verification of open- and closed-loop controlled converters. Section IV illustrates the proposed algorithms with several examples, and compares their performance with Monte Carlo analyses. Section V discusses extensions to this work, and concluding remarks are presented in Section VI.

II. Preliminaries

The basic model of a power electronics converter adopted throughout the paper is introduced, and reachability analysis concepts for switched-linear systems are presented. While different methods exist to solve the reachability problem (see, e.g., [18], [19], [20], [21] and the references therein), this work focuses on the application of ellipsoidal-based reachability analysis techniques. Ellipsoidal techniques for reachability analysis of linear systems are discussed in [22], [23], [24], [25]. Their application to hybrid systems is discussed in [26].

A. The Basic Model

A *switched system* is defined as a continuous-time system with discrete (isolated) switching events, and its dynamics can be described by a state-space model [27]. In general, power electronics converters can be thought of as switched systems, and a large class of converters can be described by a linear-switched state-space model of the form

$$\frac{dx}{dt} = A_\sigma x + B_\sigma w + E_\sigma u, \tag{1}$$

where $x(t) \in \mathbb{R}^n$ are the state variables, $w(t) \in \mathbb{R}^m$ and $u(t) \in \mathbb{R}^l$ are the system inputs; the function $\sigma : [0, \infty) \to \mathcal{Q}$, called the switching signal[1], indicates the active subsystem at every time; $\mathcal{Q}$ is called the "index set", and A_q, B_q, with $q \in \mathcal{Q}$, define the subsystems in (1). The input w is assumed to be an unknown and uncontrolled disturbance, whereas the input u is assumed to be known. In order to avoid excessive notation, we denote the valuations of the function $w(t)$ (resp. $x(t)$) simply be w (resp. x) and the implied meaning should be clear from the context.

For the uncontrolled disturbance input $w(t)$, we consider an unknown-but-bounded uncertainty model

$$w(t) \in \mathcal{W} \subseteq \mathbb{R}^m \text{ for each } t \in [0, \infty), \tag{2}$$

where $\mathcal{W}$ is a compact set contained in $\mathbb{R}^m$. For example, $\mathcal{W}$ could be a symmetric polytope, with each entry of w assumed to lie within some interval.

We want to compute the set that contains all possible values of state trajectories $x(t)$, at each t that arise from some initial condition x_0, every bounded measurable function w in (2), and all possible switching signals. This set, denoted by $\mathcal{R}$, is known in the control literature as the *reach set* or *attainability domain*. The computation of $\mathcal{R}$ determines whether the system violates performance requirements that impose bounds on the maximum excursions of certain state variables.

The exact computation of $\mathcal{R}$ is a difficult problem in general; however, some analytical techniques allow for the calculation of $\mathcal{R}$ when the set $\mathcal{W}$ is an ellipsoid. When the shape of $\mathcal{W}$ is arbitrary, it can be bounded by an ellipsoid $\Omega_w \subseteq \mathbb{R}^m$, such that $\mathcal{W} \subseteq \Omega_w$:

$$w(t) \in \Omega_w = \left\{ w \in \mathbb{R}^m : (w - w_c)' Q^{-1} (w - w_c) \leq 1 \right\}, \tag{3}$$

where $w_c \in \mathbb{R}^m$ is the center of the ellipsoid, and $Q \in \mathbb{R}^{m \times m}$ is a positive definite matrix that describes the ellipsoid's shape. If Ω_w is used instead of $\mathcal{W}$, an outer-bound approximation[2] of the exact reach set of (1) is obtained, and the question that remains is how close this outer-bound approximation is to the exact $\mathcal{R}$. One way to assess this is by computing an inner-bound approximation of the reach set and compare it with the outer-bound approximation. As it turns out, $\mathcal{W}$ is usually a symmetric polytope, which can be approximated to a high degree of precision by the union of a family of ellipsoids. When several ellipsoids are used to inner bound $\mathcal{W}$, an inner-bound approximation to the reach set $\mathcal{R}$ will result from each ellipsoid inner bounding $\mathcal{W}$. The union of these inner-bounding approximations of $\mathcal{R}$ will yield an inner-bound approximation of the reach set $\mathcal{R}$ that can be used to assess the accuracy of the outer-bound approximation. To simplify subsequent developments, $\mathcal{W}$ is assumed to be an ellipsoid (we will denote this ellipsoidal-shaped input set by Ω_w instead of $\mathcal{W}$). The remainder of this section discusses ellipsoidal-based reachability analysis techniques for switched-linear systems. In Section IV, using the ideas above, we illustrate how ellipsoidal-based reachability analysis techniques can be extended to more realistic cases when $\mathcal{W}$ is a symmetric polytope.

[1] A switching signal, as defined in [27], is a piecewise constant and everywhere right-continuous function that has a finite number of discontinuities t_i, which we call *switching times*, on every bounded time interval and thus $\sigma(t) = q \in \mathcal{Q}$, $\forall\, t \in [t_i, t_{i+1})$.

[2] A set $\mathcal{A}$ is said to be an outer-bound (inner-bound) approximation of $\mathcal{B}$ if $\mathcal{B} \subseteq \mathcal{A}$ ($\mathcal{A} \subseteq \mathcal{B}$).

B. Reachability of Switched-Linear Systems

Consider a switched-linear system with initial conditions and unknown inputs bounded by ellipsoids:

$$\begin{aligned} \tfrac{dx}{dt} &= A_\sigma x + B_\sigma w + E_\sigma u, \\ x(0) \in \Omega_x(0) &= \left\{x \in \mathbb{R}^n : (x-x_0)' P^{-1} (x-x_0) \le 1\right\}, \\ w(t) \in \Omega_w &= \left\{w \in \mathbb{R}^m : (w-w_c)' Q^{-1} (w-w_c) \le 1\right\}, \end{aligned} \quad (4)$$

where $x(t) \in \mathbb{R}^n$, $w(t) \in \mathbb{R}^m$ is unknown-but-bounded, $u(t) \in \mathbb{R}^l$ is known, $\sigma : [0,\infty) \to \mathcal{Q}$; and A_q, B_q, with $q \in \mathcal{Q} = \{0,1,2,\dots\}$ define the subsystems in (4). The events triggering the switching actions play a key role in the reach set calculation. If the switching actions depend solely on elapsed time and not the system state trajectories, then the reachability problem can be solved in a piece-wise manner using techniques for linear systems [24], [25]. In the context of power electronics, this time-based switching is typical of open-loop systems. However, switching might be both time- and state-dependent, as is typical in closed-loop control schemes. In the following, we outline the solution for the case of time-based switching; the solution to the state-based switching case is discussed in Section III.

Let $\Omega_x(t)$[3] denote the exact reach set of the system in (4) that contains all possible values of $x(t)$, and let $\eta \in \mathbb{R}^n$ be a unit vector, i.e, $\eta'\eta = 1$. Then, if every subsystem in (4) is controllable[4], $\Omega_x(t)$ can be obtained by taking the intersection of a family of outer bounding ellipsoids $\mathcal{X}_\eta$, $\forall \eta$, as follows

$$\begin{aligned} \Omega_x(t) &= \bigcap_\eta \mathcal{X}_\eta(t), \ \forall \eta \in \mathbb{R}^n, \ \text{such that } \eta'\eta = 1, \\ \mathcal{X}_\eta(t) &= \left\{x \in \mathbb{R}^n : (x-x_c)' \Psi_\eta^{-1} (x-x_c) \le 1\right\}, \\ \frac{d\Psi_\eta}{dt} &= A_\sigma \Psi_\eta + \Psi_\eta A_\sigma' + \beta_\eta(t)\Psi_\eta + \frac{1}{\beta_\eta(t)} B_\sigma Q B_\sigma', \\ \beta_\eta(t) &= \sqrt{\frac{\eta' e^{A_\sigma(t-t_i)} B_\sigma Q B_\sigma' e^{A_\sigma'(t-t_i)} \eta}{\eta' \Psi_\eta(t) \eta}}, \\ \Psi_\eta(0) &= P, \\ \frac{dx_c}{dt} &= A_\sigma x_c + B_\sigma w_c + E_\sigma u, \ x_c(0) = x_0, \end{aligned} \quad (5)$$

where t_i is the last switching instant when $A_{\sigma(t_i)}$ was activated. For each subsystem in (4), the result in (5) can be derived from Pontryagin's maximum principle [25]. For each η, the positive-definite matrix Ψ_η in (5) describes the shape of the ellipsoid $\mathcal{X}_\eta$ with center x_c, which is obtained according to the last line in (5) by setting the initial conditions to x_0 (the center of the ellipsoid $\Omega_x(0)$ that describes the set of possible initial conditions) and by setting the input disturbance to w_c (the center of the ellipsoid Ω_w that describes the set of all possible input disturbances).

Example 1: Consider the RLC circuit of Fig. (1), where

$$\begin{aligned} \frac{d}{dt}\begin{bmatrix} v_c \\ i_L \end{bmatrix} &= \begin{bmatrix} 0 & \frac{1}{C} \\ -\frac{1}{L} & -\frac{R}{L} \end{bmatrix} \begin{bmatrix} v_c \\ i_L \end{bmatrix} \\ &+ \begin{bmatrix} -\frac{1}{C} \\ 0 \end{bmatrix} i_{load} + \begin{bmatrix} 0 \\ \frac{1}{L} \end{bmatrix} V_s, \end{aligned} \quad (6)$$

[3]We reserve the use of $\mathcal{R}$ to denote the reachable set of a dynamical system with an arbitrary input set denoted by $\mathcal{W}$.

[4]A linear system $\frac{dx}{dt} = Ax + Bu$, with $x \in \mathbb{R}^n$ is controllable if and only if the controllability matrix $\mathcal{C} = \begin{bmatrix} B & AB & A^2B & \dots & A^{n-1}B \end{bmatrix}$ is full rank.

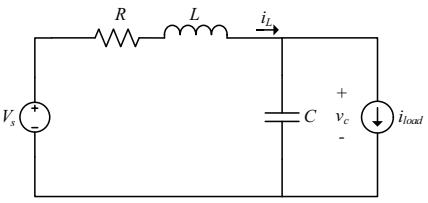

Fig. 1. RLC circuit.

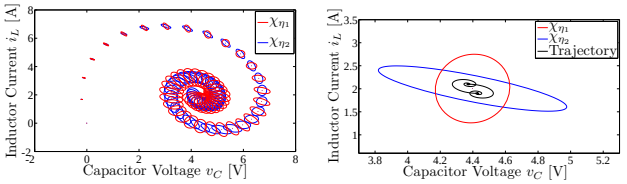

(a) Evolution of ellipsoidal bounds. (b) Steady-state bounding ellipsoids and sample trajectory for worst-case load variation.

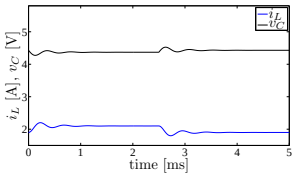

(c) Time-domain response to worst-case load variation.

Fig. 2. RLC circuit ellipsoidal bounds, sample trajectory and corresponding time-domain response.

with $R = 0.3\ \Omega$, $L = 50\ \mu$H, and $C = 100\ \mu$F. The voltage source V_s is assumed to take a constant value of 5 V, whereas the load current is assumed to vary ± 0.1 A around a nominal value of 2 A, i.e., $i_{load} \in [1.9\text{ A}, 2.1\text{ A}]$. This is a particular case of (4), where the number of subsystems is only one, i.e., $\mathcal{Q} = \{0\}$, with corresponding matrices A_0, B_0, and E_0 described in (6). Following the notation in (4), $x = [v_C, i_L]'$, $w = i_{load}$, and $u = V_s$. The unknown-but-bounded load current model can be rewritten as $|i_{load} - 2| \le 0.1$, which is equivalent to $(i_{load} - 2)^2 \le 0.01$. Therefore, following the notation in (4), this results in $Q = 0.01$, and $w_c = 2$ A. In this case, it is assumed that the initial conditions are perfectly known and equal to zero; therefore $P \in \mathbb{R}^{2\times 2}$ is a zero matrix, and $x_0 = [0,\ 0]'$. Then, by solving (5) for $\eta = [1, 0]' =: \eta_1$ and $\eta = [0, 1]' =: \eta_2$, we can obtain two different ellipsoids $\mathcal{X}_{\eta_1}(t)$ and $\mathcal{X}_{\eta_2}(t)$ at each time t that bound the reach set of (6). Figure 2(a) shows the evolution in the state space of these two bounding ellipsoids from initial conditions to steady state. The state variable values arising from all possible realizations of i_{load} are contained within the intersection of these bounding ellipsoids as they evolve in time. Figure 2(b) shows the steady-state ellipsoids, the intersection of which contains the exact steady-state reach set in addition to a worst-case load variation trajectory (the corresponding time-domain response is shown in Fig. 2(c)). The steady-state reach set is invariant in the sense that every trajectory that starts within this set will remain inside it, due to the input-to-state stability property [28]. □

III. Algorithms for Power Electronics Reachability Analysis

As previously stated, the solution to the reachability problem of the switched-linear system of (4) associated to a particular power electronics converter depends on the control strategy. In this section, we provide algorithms for solving the reachability problem in power electronics converters with open- and closed-loop control.

A. Open-loop Control

Open-loop control is carried out by operating the switching devices at fixed intervals of time in order to achieve some desired output voltage(s) and/or current(s). For example, the switching function for a power electronics converter with m configurations (i.e., $q \in \mathcal{Q} = \{0, 1, \cdots, m-1\}$) could be given by

$$\sigma(t) = \begin{cases} 0, & kT \leq t < (k+d_0)\,T \\ 1, & (k+d_0)\,T \leq t < (k+d_0+d_1)\,T \\ \cdots & \\ m-1, & \left(k + \sum_{i=0}^{m-2} d_i\right) T \leq t < (k+1)\,T, \end{cases} \tag{7}$$

where k is a nonnegative integer, T is the switching period, and d_i is the fraction of the switching period spent in the i^{th} configuration. For a converter with only two configurations, $d_0 = d$ and $d_1 = 1 - d$ where d is typically referred to as *duty-ratio*. Algorithm 1 provides an upper bound $\Omega_{x,b}(t)$ on the reach set $\Omega_x(t)$ of a converter with the open-loop control specified in (7). It is important to note that the η's belong to a predefined finite set S, whose elements are of unit length. When the algorithm ends, the intersection of the ellipsoids $\mathcal{X}_\eta(t)$ that result from each η is an upper bound to the exact reach set $\Omega_x(t)$, i.e., $\Omega_x(t) \subseteq \Omega_{x,b}(t) = \bigcap_\eta \mathcal{X}_\eta(t)$.

Algorithm 1: Open-loop reach set computation.

start
  for $i = 1$ to size(S) **do**
    $k = 0$, $\eta = S(i)$, $\Psi_\eta(0) = P$,
    repeat
      $\sigma = 0$
      compute $\mathcal{X}_\eta(t)$ for $t \in [kT,\ kT + d_0 T)$ from (5)
      for $\sigma = 1$ to $m-1$ **do**
        compute $\mathcal{X}_\eta(t)$ for
        $t \in [kT + \sum_{i=0}^{\sigma-1} d_i T,\ kT + \sum_{i=0}^{\sigma} d_i T)$ from (5)
      end for
      $k = k + 1$
    until $\mathcal{X}_\eta(t) = \mathcal{X}_\eta(t-T)$
  end for
  $\Omega_{x,b}(t) = \bigcap_\eta \mathcal{X}_\eta(t)$
end

Algorithm 1 assumes that the duty ratios remain constant for each switching period. However, duty ratios are permitted to vary from switching period to switching period. Thus, the algorithm can be easily extended to cases in which the values of d_i may vary over time, assuming these values change as a known function of the switching period. For example, a converter may have one set of d_i values during startup and another set of d_i values for steady-state operation.

B. Closed-loop Control

Closed-loop control is carried out by using state feedback to compute the switching function value. A general closed-loop control law for a power electronics converter is given by

$$\sigma(x,t) = f(x,t), \tag{8}$$

where $f : \mathbb{R}^n \times \mathbb{R} \to \mathcal{Q}$, with $\mathcal{Q}$ indexing the converter configurations. All closed-loop control laws of the form given in (8) may be described by some (possibly time-varying) switching surface G in the converter state space. The converter state variables' position in the state space in relation to the switching surface determines the active subsystem in (1), and a switch action occurs when the state trajectory crosses the switching surface. For example, a PWM controller for a converter with two possible configurations may have the form

$$\sigma(x,t) = H\left[K'\left(x_{ref} - x\right) - \Delta_{tri}(t, T_s)\right], \tag{9}$$

where $H[\cdot]$ is the Heaviside step function, x is a vector containing the converter state variables, x_{ref} is the desired system operating point, K is a gain vector, and $\Delta_{tri}(t, T_s)$ is a periodic sawtooth wave with period T_s [2]. For this case, the switching surface is linear and moves as time evolves due to the triangular wave component.

For simplicity, the formulation is limited to converters with two possible switching configurations and a closed-loop control that uses only static linear time-invariant switching surfaces. In this case, the switching function is solely a function of the converter state variables:

$$\sigma(x) = H\left[K'\left(x_{ref} - x\right)\right] = \begin{cases} 0, & K'\left(x_{ref} - x\right) \leq 0, \\ 1, & K'\left(x_{ref} - x\right) > 0, \end{cases} \tag{10}$$

This type of closed-loop control is typically referred to as *boundary control* [2]. To avoid ambiguity in the value of σ at $t = 0$, we assume that $\forall x_1, x_2 \in \Omega_{x,b}(0)$, $\sigma(x_1) = \sigma(x_2)$.

Algorithm 2 provides a method to compute an approximation of the reach set of the closed-loop controlled converter specified in (10). As in Algorithm 1, the bounding ellipsoids $\mathcal{X}_\eta$ are computed for each η contained in S. At the end of the algorithm, the intersection of the bounding ellipsoids gives $\Omega_{x,b}(t)$, an upper bound to the exact reach set $\Omega_x(t)$.

Some controllers use multiple switching surfaces, and in other cases, devices within the circuit introduce additional switching surfaces (e.g., discontinuous conduction mode). Algorithm 2 can be extended to these cases as shown in Section IV.

Algorithm 2: Closed-loop reach set computation.

start
  $k = 0$, $t_k = 0$
  compute σ from (10)
  for $i = 1$ to size(S) **do**
    $\eta = S(i)$
    $\Psi_\eta(t_k) = P$
    compute $\mathcal{X}_\eta(t)$ from (5)
  end for
  repeat
    $\Omega_{x,b}(t) = \bigcap_\eta \mathcal{X}_\eta(t)$
    $\Phi(t) = \bigcup_{j\in[0,t]} \Omega_{x,b}(j)$
    $\mathcal{Y}(t) = \Phi(t) \bigcap G$
    if $\Omega_{x,b}(t)$ completely passes through G **then**
      compute σ from (10)
      $t_k = t$
      for $i = 1$ to size(S) **do**
        $\eta = S(i)$
        pick $\Psi_\eta(t_k)$ such that $\mathcal{X}_\eta(t_k) \supseteq \mathcal{Y}(t)$
        compute $\mathcal{X}_\eta(t)$ from (5)
      end for
      $\mathcal{Y}(t) = \emptyset$
      $k = k + 1$
      $\Omega_{x,b}(t) = \bigcap_\eta \mathcal{X}_\eta(t)$
    end if
  until $\Omega_{x,b}(t_{k-2}) = \Omega_{x,b}(t_k)$, $\Omega_{x,b}(t_{k-3}) = \Omega_{x,b}(t_{k-1})$
end

C. Choice of Unit Vectors η that Comprise the Set S

The accuracy of the reach set approximation depends on the choice of the η vectors in S. Although in theory an infinite number of unit vectors are needed to obtain the exact reach set, in practice, it suffices to choose a few η's in order to obtain an accurate approximation. A good rule-of-thumb is to choose the unit vectors that define each axis direction. Thus, if $x \in \mathbb{R}^n$, $S = \{\eta_1, \eta_2, \ldots, \eta_n\}$, where the i^{th} entry of η_i, $\forall i = 1, 2, \ldots, n$ is one, and the other entires are zero. In all the examples discussed later involving DC-DC converters, $n = 2$, and thus $S = \{[1, 0]', [0, 1]'\}$. An appealing feature is that, in Algorithms 1 and 2, the "for" loop involving the elements in S can be parallelized. Additionally, the objective of the analysis might be to just verify whether the reach set $\mathcal{R}$ is contained within a region of the state-space defined by performance requirements. If for a particular η_i, the resulting outer-bound ellipsoidal approximation $\mathcal{X}_{\eta_i}$ is contained within the state-space region defined by performance requirements, then it can be concluded that the exact reach set will be within the tolerance region without further analysis.

IV. Application Examples

This section illustrates some applications of the algorithms introduced in Section III to verify the large-signal behavior of buck and boost converters under different control strategies.

TABLE I
Open-loop controlled buck converter parameters.

Parameter	Value
R_L [Ω]	0.1
R_C [Ω]	5e-2
L [H]	12e-6
C [F]	6e-4
f [kHz]	250
d	0.45
V_c [V]	12
Q_v [V]	0.1
I_c [A]	4
Q_i [A]	1
λ [%]	7.5
V_{ref} [V]	5

We assume that the voltage supply and/or the current load can vary within certain bounds. We evaluate if voltage regulation requirements are met for every possible trajectory that results from all possible voltage supply and/or load variations. Algorithm performance is compared to Monte Carlo analysis. The Ellipsoidal Toolbox [29] is used for reach set computations, and PLECS [30] is used for time-domain simulations.

A. Open-Loop Controlled Buck Converter

Consider the buck converter in Fig. 3, where R_L is the DC resistance of the inductor, and R_C is the capacitor equivalent series resistance (ESR). The load is modeled as a current source and open-loop control with fixed duty ratio d is assumed. The system states are the capacitor voltage v_C, and inductor current i_L, i.e., $x = [v_C, i_L]'$. It is assumed that both voltage supply source V_s and load current i_{load} are unknown-but-bounded, i.e., $w = [V_s, i_{load}]'$, taking on values in a set $\mathcal{W}$ defined by

$$\mathcal{W} = \{[V_s, i_{load}]' : |V_s - V_c| \le Q_v,\ |i_{load} - I_c| \le Q_i\}, \quad (11)$$

where V_c, I_c represent the nominal values of V_s and i_{load}, and Q_v, Q_i represent the corresponding magnitude of variations.

In continuous conduction mode, this converter can be described by a switched-linear model consisting of two different subsystems. Following the notation in (1), the matrices describing the system dynamics for each subsystem are

$$A_0 = \begin{bmatrix} 0 & \frac{1}{C} \\ -\frac{1}{L} & -\frac{R_L+R_C}{L} \end{bmatrix},\ B_0 = \begin{bmatrix} 0 & -\frac{1}{C} \\ 0 & \frac{R_C}{L} \end{bmatrix},$$
$$A_1 = \begin{bmatrix} 0 & \frac{1}{C} \\ -\frac{1}{L} & -\frac{R_L+R_C}{L} \end{bmatrix},\ B_1 = \begin{bmatrix} 0 & -\frac{1}{C} \\ \frac{1}{L} & \frac{R_C}{L} \end{bmatrix}. \quad (12)$$

It is important to note that E_0 and E_1 do not appear in this example because all inputs are assumed to be unknown.

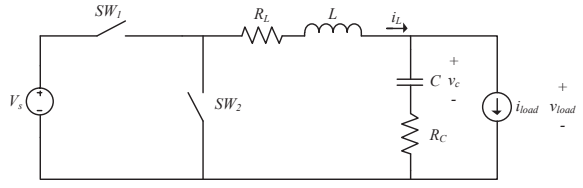

Fig. 3. Buck converter schematic.

TABLE II
ENTRIES OF SHAPE MATRIX Q DEFINING Ω_1, Ω_{2a}, Ω_{2b}, AND Ω_{2c}.

	q_{11}	$q_{12} = q_{21}$	q_{22}
Ω_1	0.02	0	1.99
Ω_{2a}	0.01	-0.063	0.99
Ω_{2b}	0.01	0.063	0.99
Ω_{2c}	0.01	0	1

1) Reachability analysis: It is conducted for converter parameters taking on the values in Table I. Controllability of each subsystem in (12) can be verified by checking that the controllability matrices[4] are full rank. Ellipsoidal-based methods cannot be directly applied since, as described in (11), the input space set is a rectangle. The solution is to to define outer- and inner-bound ellipsoids to the input set.

Outer-bound approximation: In Fig. 4(a), the input space $\mathcal{W}$ is outer-bounded by a minimum volume ellipsoid Ω_1. The entries of the shape matrix Q defining Ω_1 are given in Table II. According to the notation used in Algorithm 1, we define $S = \{\eta_1, \eta_2\}$, with $\eta_1 = [1,\ 0]'$ and $\eta_2 = [0,\ 1]'$; and run it for the input set Ω_1. Figure 4(b) shows the two sets of outer-bounding ellipsoids $\mathcal{X}_{\eta_1,1}$ and $\mathcal{X}_{\eta_2,1}$ at selected time instants during a switching period. An upper bound to the set of reachable states at a particular time instant is given by the intersection of the corresponding two ellipsoids. The union of these intersections over all times gives an outer bound to the set of reachable states over the entire switching period. Figure 4(b) also shows the converter trajectory resulting from an input change of $w = [11.9\text{ V},\ 5\text{ A}]'$ to $w = [12.1\text{ V},\ 3\text{ A}]'$ and vice versa. As expected, this trajectory is contained within $\bigcup_t \left(\mathcal{X}_{\eta_1,1}(t) \bigcap \mathcal{X}_{\eta_2,1}(t)\right)$.

Inner-bound approximation: In Fig. 5(a), the input space is inner-bounded by three ellipsoids, Ω_{2a}, Ω_{2b}, and Ω_{2c}. In this case, an inner-bound approximation of the reach set can be computed from each input ellipsoid Ω_{2a}, Ω_{2b}, and Ω_{2c}, and the union of these three reach set approximations gives an inner bound to the exact reach set. The entries of the shape matrix Q defining Ω_{2a}, Ω_{2b}, and Ω_{2c} are given in Table II. We run Algorithm 1 with the same η's used before for each ellipsoid Ω_{2a}, Ω_{2b}, and Ω_{2c}. The resulting pairs of reach set inner-bound ellipsoids are displayed in Fig 5(b), Fig 5(c), and Fig 5(d), respectively. The intersection of each pair yields an inner-bound approximation, and the union of these inner-bound approximations results in a more accurate inner-bound reach set approximation.

Figure 6(a) displays the outer-bound ellipsoid and all three inner-bound ellipsoids at some time instant when $\sigma = 1$. Figure 6(b) displays the corresponding intersections, denoted by $\Omega_{x,b1}$, and $\Omega_{x,b2}$ respectively, of the outer- and inner-bound ellipsoids in Fig. 6(a).

2) Voltage regulation verification: It is assumed that design requirements impose load voltage v_{load} to be within an acceptable tolerance specified by

$$|v_{load} - V_{ref}| \leq \lambda V_{ref}, \tag{13}$$

where V_{ref} is the desired load voltage and $\lambda > 0$ is a constant known as *voltage regulation* [3].

The load regulation requirement is given in terms of v_{load}, not in terms of v_C. Thus, once the reach set $\mathcal{R}$ is obtained (in the v_C -i_L space), it is necessary to map it onto the v_{load}-space through a series of set transformations described next. The graphical interpretation of these transformations is shown in Fig. 7. First, note that

$$v_{load} = v_C + R_C(i_L - i_{load}) = [1, R_C]x - R_C i_{load}. \tag{14}$$

Define $y = [1, R_C]x$, and denote $\mathcal{P}_y$ as the projection of $\mathcal{R}$ onto the direction defined by the unit vector $e = \frac{1}{\sqrt{1+R_C^2}}[1, R_C]'$. Then y will belong to an interval $\mathcal{S}_y$, which results from scaling $\mathcal{P}_y$ by the factor $\sqrt{1+R_C^2}$ [22]:

$$\begin{aligned} y \in \mathcal{S}_y &= \{y : y = \sqrt{1+R_C^2}\hat{y},\ \hat{y} \in \mathcal{P}_y\}, \\ &= \{y : y \in [y_{min}, y_{max}]\}. \end{aligned} \tag{15}$$

Since i_{load} is unknown-but-bounded, as described in (11), then v_{load} belongs to an interval set described by

$$v_{load} \in \mathcal{V} = \{v_{load} : v_{load} = y - R_C i_{load}\}, \tag{16}$$

where $y \in [y_{min}, y_{max}]$, and $i_{load} \in [I_C - Q_i, I_C + Q_i]$. Finally, it follows from (14), (15), and (16) that

$$y_{min} - R_C(I_C + Q_i) \leq v_{load} \leq y_{max} - R_C(I_C - Q_i). \tag{17}$$

Therefore, the regulation requirement is met if and only if

$$\begin{aligned} y_{min} - R_C(I_C + Q_i) &\geq (1-\lambda)V_{ref}, \\ y_{max} - R_C(I_C - Q_i) &\leq (1+\lambda)V_{ref}. \end{aligned} \tag{18}$$

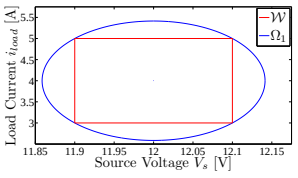

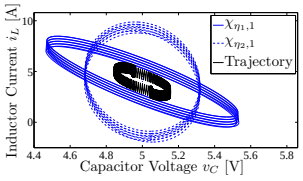

(a) Input space $\mathcal{W}$ and outer-bound ellipsoidal approximation Ω_1.

(b) Reach set outer-bound ellipsoids $\mathcal{X}_{\eta_1,1}$ and $\mathcal{X}_{\eta_2,1}$, and trajectory.

Fig. 4. Outer-bound approximation for open-loop controlled buck converter: input space and reach set approximation.

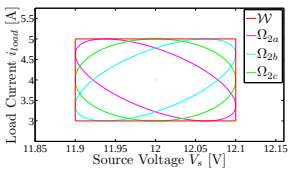

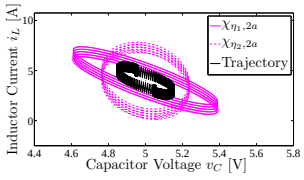

(a) Input space $\mathcal{W}$ and inner-bound ellipsoids Ω_{2a}, Ω_{2b}, and Ω_{2c}.

(b) Reach set inner-bound ellipsoids $\mathcal{X}_{\eta_1,2a}$ and $\mathcal{X}_{\eta_2,2a}$, and trajectory.

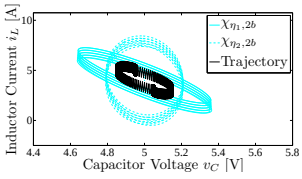

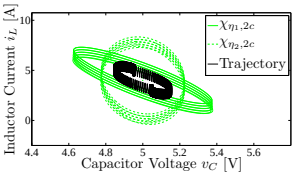

(c) Reach set inner-bound ellipsoids $\mathcal{X}_{\eta_1,2b}$ and $\mathcal{X}_{\eta_2,2b}$, and trajectory.

(d) Reach set inner-bound ellipsoids $\mathcal{X}_{\eta_1,2c}$ and $\mathcal{X}_{\eta_2,2c}$, and trajectory.

Fig. 5. Inner-bound approximation for open-loop controlled buck converter: input space and reach set approximation.

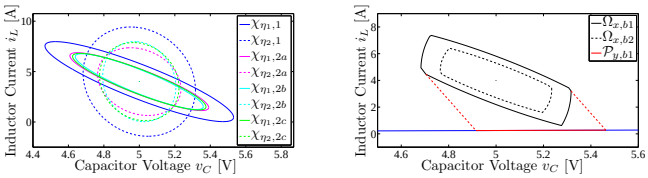

(a) Inner- and outer-bound ellipsoids. (b) Intersection of inner- and outer-bound ellipsoids and projection $\mathcal{P}_{y,b1}$[5] for a fixed time when $\sigma = 1$.

Fig. 6. Open-loop controlled buck converter: inner- and outer-bound reach set approximations, and corresponding intersections at a fixed time for $q = 1$.

The conditions given in (18) also apply to all other examples discussed later in this section.

The projection of the range of $\Omega_{x,b1}$ onto the subspace defined by $e = \frac{1}{\sqrt{1+R_C^2}}[1, R_C]' = [0.99, 0.05]'$, denoted by $\mathcal{P}_{y,b1}$, is displayed in Fig. 6(b)[5]. Following the notation in (15), $\mathcal{S}_{y,b1}$ is given as $[4.93, 5.48]$. From (17), it follows that $4.68 \leq v_{load} \leq 5.33$. From (18), we conclude that v_{load} meets the $\pm 7.5\%$ voltage regulation requirement.

Choice of outer- or inner-bound input ellipsoids: It depends on the objective of the analysis. If a single minimum-volume, outer-bound, input ellipsoid results in an outer-bound reach set approximation that is contained within the region of the state space defined by performance requirements, then we can conclude that any input contained in the input space will result in system trajectories that meet performance requirements. Otherwise, no conclusion can be made. The use of several inner-bound input ellipsoids will yield an inner-bound approximation of the reach set. If this approximation is not contained within the requirements region, then we can conclude that that there are inputs that result in trajectories not meeting performance requirements. Using multiple inner-bound input ellipsoids improves the accuracy of the reach set approximation, at the expense of computation time.

B. Closed-Loop Controlled Buck Converter

Consider the buck converter in Fig. 3 operating in closed-loop with a static linear switching boundary of the form

$$\sigma(x) = H\left[K'\left(x_{ref} - x\right)\right], \tag{19}$$

with $K = [k_v,\ k_i]'$, where k_v and k_i are the controller voltage and current gains respectively, $x_{ref} = [V_{ref},\ I_{ref}]'$, where V_{ref} is the desired load voltage, and I_{ref} is the desired current

[5]Although in the figure the dotted parallel lines do not appear perpendicular to the line where the projection $\mathcal{P}_{y,b1}$ is defined, in reality they are. This is just a skewing effect due to different axis scales.

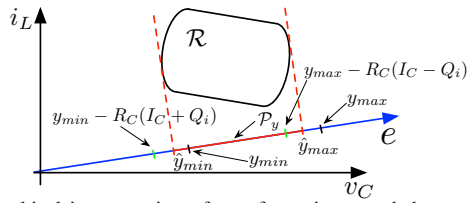

Fig. 7. Graphical interpretation of transformations needed to verify voltage regulation requirements.

TABLE III
CLOSED-LOOP BUCK CONVERTER PARAMETERS.

Parameter	Value
R_L [Ω]	10e-3
R_C [Ω]	5e-2
L [H]	50e-6
C [F]	44.1e-6
V_c[V]	12
Q_v [V]	1
I_c [A]	2
Q_i [A]	2
I_{ref} [A]	4
k_v	100
k_i	25
λ [%]	5
V_{ref}[V]	5

through the inductor. As in the open-loop case, it is assumed that the load current i_{load} and input voltage V_s are unknown-but-bounded, i.e., $w = [V_s, i_{load}]'$, and the values they take are defined, as in the open-loop case by (11), where V_C, Q_v, I_c, and Q_i, are constants taking on the values in Table III.

In this case, SW_2 is implemented by a diode, and it is assumed that the converter parameters are such that the converter is operating in discontinuous current mode (DCM). This introduces a third configuration (SW_1 and SW_2 both open), i.e., $\mathcal{Q} = \{0,\ 1,\ 2\}$. Then, following the notation in (1), the matrices describing $q = 0$, and $q = 1$, are the same as in (12), and the matrices describing $q = 2$, corresponding to DCM, are

$$A_2 = \begin{bmatrix} 0 & \frac{1}{C} \\ 0 & 0 \end{bmatrix},\ B_2 = \begin{bmatrix} 0 & -\frac{1}{C} \\ 0 & 0 \end{bmatrix}. \tag{20}$$

Design requirements impose the same voltage regulation defined as in (13) for the open-loop converter, with λ and V_{ref} taking on the values in Table III.

1) Reachability analysis: This was conducted for the converter model defined in (19)—(20), with parameters taking on the values in Table III. The subsystem corresponding to the discontinuous conduction mode is not controllable as the rank of the controllability matrix[4] for this mode is 1. However, with a simple understanding of the converter trajectories in DCM, it is clear that the reach set may still be computed. A slight

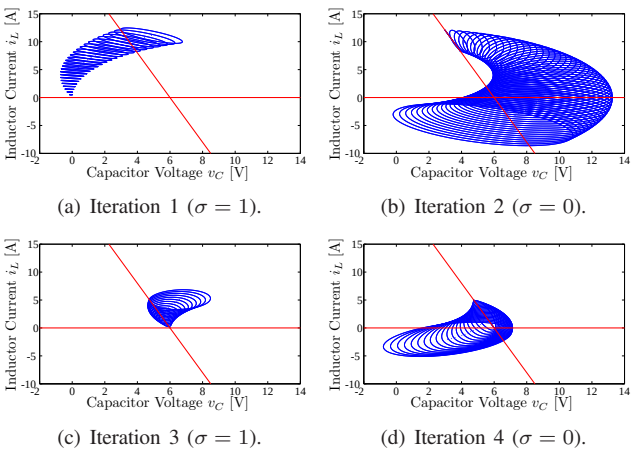

(a) Iteration 1 ($\sigma = 1$). (b) Iteration 2 ($\sigma = 0$).

(c) Iteration 3 ($\sigma = 1$). (d) Iteration 4 ($\sigma = 0$).

Fig. 8. Reach set evolution of closed-loop controlled buck converter.

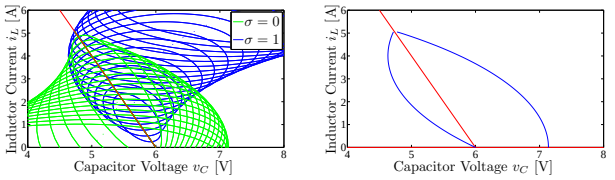

(a) Steady-state ellipsoids evolution. (b) Reach set outline.

Fig. 9. Steady-state reach set for closed-loop controlled buck converter in DCM operation.

modification to Algorithm 2 must be made to account for the DCM switching boundary. This region of operation may be handled by introducing an additional switching surface on the zero current axis. Once the converter is in DCM, the inductor current i_L will remain zero while the capacitor voltage v_C decreases as the capacitor discharges to supply the load. Thus, once the system state trajectory intersects the zero current axis, the trajectory will remain on the zero current axis and move toward the origin. This behavior will continue until the state trajectory crosses the switching surface G and switch SW_1 turns on. In this regard, when computing the set of reachable states, it is sufficient to simply remove the set of points that fall below the zero current axis from $\Phi(t)$ (the set containing the union of the bounding ellipsoids) at the end of each computation performed for $\sigma = 0$. If the entire set $\Phi(t)$ is below the zero current axis, then $\Psi_\eta(\tau)$ is reset to a value such that $\mathcal{X}_\eta(\tau) \supseteq \mathcal{Y}(\tau)$, where $\mathcal{Y}(\tau)$ is the intersection of $\Phi(\tau)$ and G.

Figure 8 shows the evolution of the reach set for the first four iterations of Algorithm 2, starting from the origin. In each figure, the switching surface G is shown by the diagonal red line and the discontinuous conduction boundary is shown by the horizontal red line on the zero current axis. It is apparent in Fig. 8(b) that the converter may enter DCM for some operating conditions. Figure 8(c) shows how the set of points in $\mathcal{Y}(\tau)$ that fall below the DCM boundary are removed at the end of each computation when $\sigma = 0$. In each figure, the bounding ellipsoids below the DCM boundary may be disregarded as this region of the state-space is unreachable.

Figure 9 displays the steady-state solution to the closed-loop reachability problem. Figure 9(a) shows the evolution of the bounding ellipsoids for each configuration when the system is in steady state. The blue ellipsoids are valid for $\sigma = 1$, i.e., to the left of G, and the green ellipsoids are valid when $\sigma = 0$, i.e., to the right of G. Figure 9(b) shows an outline of the region in which the bounding ellipsoids are valid. In the figure, the set of reachable states $\Omega_x(t)$ for this converter in steady-state operation is the region enclosed by the blue traces and the zero current axis.

2) Voltage regulation verification: It is apparent from Fig. 9(b) that the $\pm 5\%$ voltage regulation requirement is not met. Thus, the design needs to be further modified to meet this requirement. In some cases, it is possible for the system to violate the performance bounds for a short period of time without jeopardizing the functionality of the system. These types of performance bounds are known as soft bounds, e.g., bounds imposed by component thermal limits. However, there also exist other cases in which a violation of a certain performance bound can cause the system to fail.

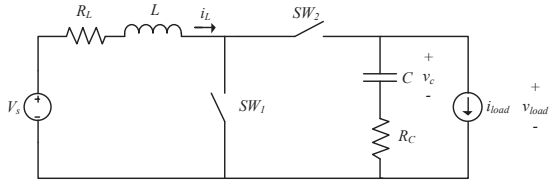

Fig. 10. Boost converter schematic.

C. Open-Loop Controlled Boost Converter

Consider the boost converter in Fig. 10. The inputs V_s and i_{load} are both considered to be unknown-but-bounded, i.e., $w = [V_s, i_{load}]'$ and the values they take on are defined as in (11). Continuous conduction mode is assumed and therefore, the matrices describing the dynamics of each subsystem are

$$A_0 = \begin{bmatrix} 0 & \frac{1}{C} \\ -\frac{1}{L} & -\frac{R_L + R_C}{L} \end{bmatrix}, \; B_0 = \begin{bmatrix} 0 & -\frac{1}{C} \\ \frac{1}{L} & \frac{R_C}{L} \end{bmatrix},$$
$$A_1 = \begin{bmatrix} 0 & 0 \\ 0 & -\frac{R_L}{L} \end{bmatrix}, \; B_1 = \begin{bmatrix} 0 & -\frac{1}{C} \\ \frac{1}{L} & 0 \end{bmatrix}. \qquad (21)$$

Algorithm 1 is used to obtain an outer-bound ellipsoidal approximation of the reach set of (21), with parameters taking on the values in in Table IV. Controllability of each individual subsystem in (21) can be easily checked[4]. As in the buck open-loop case, we bound the input set with a single outer-bound minimum volume ellipsoid Ω_w centered at $[V_c, I_c]'$. The entries of the shape matrix Q corresponding to Ω_w are $q_{11} = 0.02$, $q_{22} = 0.12$, and $q_{12} = q_{21} = 0$.

TABLE IV
OPEN-LOOP BOOST CONVERTER PARAMETERS.

Parameter	Value
R_L [Ω]	0.2
R_C [Ω]	5e-2
L [H]	50e-6
C [F]	200e-6
f [kHz]	200
d	0.79
V_c [V]	12
Q_v [V]	0.1
I_c [A]	2
Q_i [A]	0.25
λ [%]	5
V_{ref}[V]	48

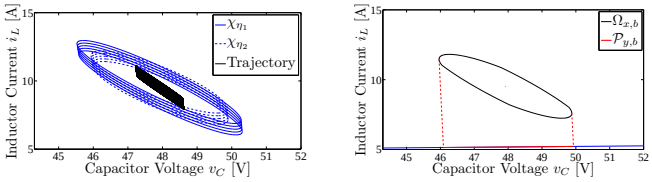

(a) Reach set outer-bound ellipsoids $\mathcal{X}_{\eta_1}$ and $\mathcal{X}_{\eta_2}$, and trajectory. (b) Intersection of $\mathcal{X}_{\eta_1,1}(\tau)$ and $\mathcal{X}_{\eta_2,1}(\tau)$ and projection $\mathcal{P}_y$[5] for a fixed time when $q = 1$.

Fig. 11. Outer-bound approximation for open-loop controlled boost converter.

1) Reachability analysis: Algorithm 1 is run for $\eta_1 = [1,\ 0]'$ and $\eta_2 = [0,\ 1]'$. Figure 11(a) shows the corresponding reach set ellipsoidal approximations $\mathcal{X}_{\eta_1}$ and $\mathcal{X}_{\eta_2}$, displayed for chosen time instants during one switching period of the converter's steady-state operation. Additionally, Fig. 11(a) shows the evolution of the converter state variables resulting from an input change of $w = [11.9\ \text{V},\ 2.25\ \text{A}]'$ to $w = [12.1\ \text{V},\ 1.75\ \text{A}]'$ and vice versa. For a fixed time τ, Fig. 11(b) shows the intersection of two ellipsoids $\mathcal{X}_{\eta_1}(\tau)$ and $\mathcal{X}_{\eta_2}(\tau)$ of Fig. 11(a).

2) Voltage regulation verification: Voltage regulation requirements are verified following the same procedure for the buck converter outlined in (14)—(18). The projection of the range of $\Omega_{x,b}$ onto the subspace spanned by $e = [0.99, 0.05]'$ is displayed in Fig. 11(b) ($\mathcal{P}_{y,b}$). Then, $\mathcal{S}_{y,b}$ is obtained according to (15) to be $[46.37, 50.20]$. It follows from (17) that $46.25 \leq v_{load} \leq 50.1$. Finally, from (18), we conclude that v_{load} meets the $\pm 5\%$ voltage regulation requirement.

D. Closed-Loop Controlled Boost Converter

Consider the boost converter in Fig. 10, where V_s is fixed and known, and i_{load} is assumed to be unknown-but-bounded, i.e., $u = V_S$ and $w = i_{load}$, and the values i_{load} can take are defined as in (11). The matrices describing converter dynamics are

$$A_0 = \begin{bmatrix} 0 & \frac{1}{C} \\ -\frac{1}{L} & -\frac{R_L + R_C}{L} \end{bmatrix},\ B_0 = \begin{bmatrix} -\frac{1}{C} \\ \frac{R_C}{L} \end{bmatrix},\ E_0 = \begin{bmatrix} 0 \\ \frac{1}{L} \end{bmatrix},$$
$$A_1 = \begin{bmatrix} 0 & 0 \\ 0 & -\frac{R_L}{L} \end{bmatrix},\ B_1 = \begin{bmatrix} -\frac{1}{C} \\ 0 \end{bmatrix},\ E_1 = \begin{bmatrix} 0 \\ \frac{1}{L} \end{bmatrix}. \quad (22)$$

The converter controller implements a hysteresis control, with a switching function given by

$$\sigma(x(t)) = \begin{cases} 0, & K'(x_{ref} - x(t)) \leq -\rho, \\ \sigma(x(t^-)), & -\rho < K'(x_{ref} - x(t)) \leq \rho, \\ 1, & K'(x_{ref} - x(t)) > \rho, \end{cases} \quad (23)$$

where $K = [k_v,\ k_i]'$, and $x_{ref} = [V_{ref},\ I_{ref}]'$, ρ is a constant that describes the hysteresis band width, and t^- denotes a time instant prior to and infinitesimally close to t. The hysteresis band may be represented in the state space as two separate switching boundaries G_1 and G_2 (solid red lines), where G_1 lies below and to the left of G_2 in the state-space. The converter then operates by activating one configuration when the state trajectory is to the left of G_1 and then switching to the other configuration when the state trajectory is to the right of G_2. When the state trajectory is between the two switching boundaries, the converter remains in its previous configuration.

1) Reachability and regulation verification: Algorithm 2 was modified to handle two switching boundaries and the analysis was performed with the converter parameters taking on values in Table V. Figure 12 shows the evolution of the reach set for both the startup (Fig. 12(a)) and steady-state (Fig. 12(b)). The converter is started with open-loop control by slowly increasing the duty ratio until the converter trajectory crosses G_1, the instant at which the converter switches from open-loop operation to hysteresis control. From Fig. 12(b), it is obvious that even after the startup phase has passed, the converter does not meet the $\pm 5\%$ voltage regulation requirement.

TABLE V
CLOSED-LOOP BOOST CONVERTER PARAMETERS.

Parameter	Value
R_L [Ω]	10e-3
R_C [Ω]	5e-2
L [H]	50e-6
C [F]	20e-6
V_s[V]	12
I_c [A]	2
Q_i [A]	0.25
I_{ref} [A]	4.27
k_v	2
k_i	10
ρ	5
λ [%]	5
V_{ref}[V]	48

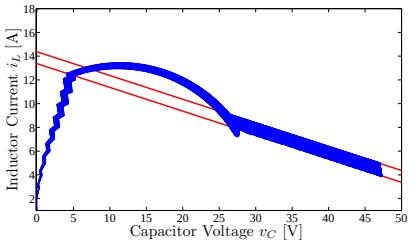

(a) Reach set during startup.

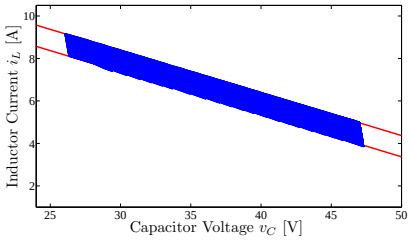

(b) Steady-state reach set.

Fig. 12. Reach set for hysteresis-controlled boost converter.

E. Comparison with Monte Carlo Analysis

The computational performance of ellipsoidal methods is compared with Monte Carlo analysis for the open- and closed-loop buck converter, and the open-loop boost. The analysis is conducted by setting the converter initial conditions to those corresponding to nominal operating conditions, and assuming that V_s and i_{load} can randomly jump at randomly chosen time instants. Simulations are conducted for 1000, and 10,000 jumps. The computation times for each experiment are listed in Table VI together with the time taken to conduct the corresponding reachability analysis. It can be seen that, in general, reachability analysis requires significantly less time than Monte Carlo analysis.

V. EXTENSIONS

In this section, we discuss two directions for extending this work. The first extension deals with the case when uncertainty in converter operation is caused by parameter variability

TABLE VI
MONTE CARLO AND REACHABILITY ANALYSIS COMPUTATION TIMES IN MIN. FOR OPEN-LOOP (O-L) AND CLOSED-LOOP (C-L) BUCK AND OPEN-LOOP BOOST.

	O-L Buck	C-L Buck	O-L Boost
1000 jumps	17.2393	36.6841	16.7065
10,000 jumps	180.6201	360.2374	169.8644
Reachability	38.0973	0.4106	38.1993

instead of input variability. The second extension modifies Algorithm 2 to accomodate for some special control strategies.

A. Unknown-but-Bounded Parametric Uncertainty

Uncertainty due to variations in parameter values affects the matrices A_q, B_q, and E_q for each subsystem in (1). The techniques introduced in this paper can be extended to address this problem.

To fix ideas, we consider the buck converter in Fig. 3, where the value that R_C takes on is uncertain except for some upper and lower bound, i.e., $R_C \in [R_C^{min}, R_C^{max}]$. Then, the values that R_C takes are described by $|R_C - \frac{R_C^{min}+R_C^{max}}{2}| \leq \frac{R_C^{max}-R_C^{min}}{2}$, which can be rewritten as

$$R_C \in \mathcal{R}_C = \{R_C : (R_C - R_C^*)^2 Q_{R_C}^{-2} \leq 1\}, \qquad (24)$$

where $R_C^* = \frac{R_C^{min}+R_C^{max}}{2}$, and $Q_{R_C} = \frac{R_C^{max}-R_C^{min}}{2}$. Let us assume for simplicity in subsequent developments that the voltage supply V_S and the load current i_{load} are both constant (including variations on both has already been discussed). Then, the matrices A_q and E_q (E_q is the same as B_q in (12), as all the inputs are known), are a function of R_C. To emphasize this dependence, we will make it explicit, i.e., $A_q(R_C)$ and $E_q(R_C)$. Then, the converter dynamics is described as

$$\begin{gathered} \tfrac{dx}{dt} = A_\sigma(R_C)x + E_\sigma(R_C)u, \\ x(0) = x_0, \\ R_C \in \mathcal{R}_C = \{R_C : (R_C - R_C^*)^2 Q_{R_C}^{-2} \leq 1\}, \end{gathered} \qquad (25)$$

where $x = [v_c, i_L]'$, and $u = [V_S, i_{load}]'$. The ellipsoidal techniques described above cannot be directly applied to (25) to obtain the reach set $\mathcal{R}$ (or an approximation), as the uncertainty does not appear as an additive disturbance. However, by linearizing each subsystem in (25) around R_C^*, we can describe the perturbations in $x(t)$ that result from perturbing R_C around R_C^*. Then, the converter reach set $\mathcal{R}$ can be approximated by the reach set $\Delta\mathcal{R}$ that results from the linearization.

Let $x(t) = x^* + \Delta x$, where x^* is the trajectory that results from the nominal conditions, and Δx denotes perturbations of the trajectory around x^* due to variations in R_C around R_C^*. Let $R_C(t) = R_C^* + \Delta R_C$, where $\Delta R_C \in \Delta\mathcal{R}_C$, and $\Delta\mathcal{R}_C$ is such that $\mathcal{R}_C = R_C^* \oplus \Delta\mathcal{R}_C$, where "$\oplus$" denotes the Minkowski sum. Then, small variations in the system trajectories, denoted by Δx, originating from small variation in R_C, denoted by ΔR_C, can be approximated by

$$\begin{gathered} \tfrac{d\Delta x}{dt} = A_\sigma^* \Delta x + B_\sigma^* \Delta R_C, \\ \Delta x(0) = 0, \\ \Delta R_C \in \Delta\mathcal{R}_C = \{\Delta R_C : \Delta R_C^2 Q_{R_C}^{-2} \leq 1\}, \end{gathered} \qquad (26)$$

where it can be easily verified that $A_\sigma^* := A(R_C^*)$, and $B_\sigma^* := \frac{\partial A_\sigma}{\partial R_C}\big|_{R_C^*} x^* + \frac{\partial E_\sigma}{\partial R_C}\big|_{R_C^*} u$. It is clear that (26) is in the form of (4) except for the fact that B_σ^* is time-varying (this is due to the fact that x^* is a function of time). However, the ellipsoidal techniques described above still apply to linear time-varying systems as discussed in [24]. Therefore, we can utilize them to obtain an approximation of the reach set of (26), which is denoted by $\Delta\mathcal{R}$. The reach set $\mathcal{R}$ of (25) can be approximated as $\mathcal{R} \approx x^* \oplus \Delta\mathcal{R}$.

B. Special Control Methods

There are many control techniques in the literature beyond the ones used in our examples. It is possible to tailor the techniques presented in this paper to particular control techniques, but the tailoring is problem-specific and limitations might arise depending on the problem.

We will illustrate an extension of Algorithm 2 for closed-loop control to a family of special control strategies referred to as rippled-based control (see, e.g., [31], [32], [33] and the references therein). In these strategies, the converter output voltage ripple is used in a PWM scheme. To fix ideas, we focus on a particular ripple-based control strategy known as V^2 control. We will show that the analysis of a V^2-controlled buck converter can be recast into a boundary-control analysis problem by augmenting the converter state-space representation to also include the controller states. Consider the buck converter of Fig. 3; then, following the V^2 scheme described in [31], the switching function can be described by

$$\sigma = H[v_m - v_r], \qquad (27)$$

where $H[\cdot]$ is the Heaviside step function. The signal v_m is the output of a linear-time invariant (LTI) system, which can be described by a transfer function $H_v(s)$ as in [31], or alternatively by a state-space model of the form

$$\begin{gathered} \dot{z} = Fz + G(V_{ref} - v_{load}), \\ v_m = Mz, \end{gathered} \qquad (28)$$

where $z \in \mathbb{R}^p$, $F \in \mathbb{R}^{p\times p}$, $G \in \mathbb{R}^{p\times 1}$, and $M \in \mathbb{R}^{1\times p}$; and V_{ref} is the load voltage reference. The signal v_r is given by

$$v_r = v_{load} + \Delta_{tri}(t, T_s), \qquad (29)$$

where $\Delta_{tri}(t, T_s)$ is a periodic sawtooth wave with period T_s. Since $v_{load} = v_c + R_C(i_L - i_{load})$, it follows from (28) that

$$\sigma = H[Mz - v_c - R_C(i_L - i_{load}) - \Delta_{tri}(t, T_s)]. \qquad (30)$$

Define $\tilde{x} = [x', z']'$, where $x = [v_C, i_L]'$, $\tilde{x}_{ref} = [0, i_{load}, 0, 0]'$, and $K = [D, -M]'$, where $D = [1, R_C]$. Then (30) can be rewritten as

$$\sigma = H[K'(\tilde{x}_{ref} - \tilde{x}) - \Delta_{tri}(t, T_s)], \qquad (31)$$

which is of the same form as (9) for the case of a PWM controller. Thus, the original V^2-controlled buck converter problem has been recast into a boundary-based control problem (with a linear moving boundary), where the state-space consists of the original converter states v_C and i_L, and the controller states z. The only non-zero entry of $\tilde{x}_{ref}$, which is

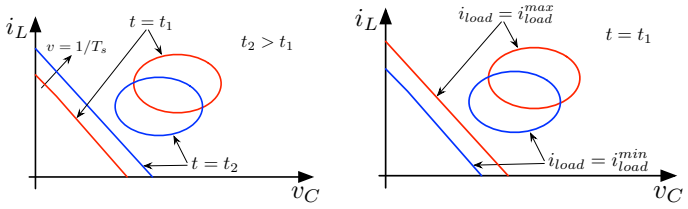

(a) Ellipsoid and moving boundary with speed $v = 1/T_s$ for two time-instants $t_2 > t_1$ and a fixed load.

(b) Ellipsoid and moving boundary for maximum and minimum loads at a fixed time $t = t_1$.

Fig. 13. Graphical interpretations of modifications needed in Algorithm 2 to account for moving boundaries and load variations.

i_{load} means that the controller will try to force i_L to follow i_{load}. If i_{load} varies as in the examples previously discussed, then the position of the moving boundary will also vary with i_{load}. Algorithm 2 can be modified to account for these two effects as follows. For the moving boundary effect (illustrated in Fig. 13(a)), as time evolves, it is only necessary to modify the position of the boundary according to the sawtooth signal $\Delta_{tri}(t, T_s)$. For the variation in i_{load} (illustrated in Fig. 13(b)), we conduct two separate reachability analysis for the moving boundary that results in fixing i_{load} to the maximum and minimum values it can take. The union of the resulting reach sets takes into account both the moving boundary effect and variations in i_{load}.

VI. Concluding Remarks

In this paper, a method for large-signal behavior verification of power electronics systems subject to bounded uncertain inputs was proposed. This method relies on the solution to the reachability problem associated with such systems, which is the computation of the reach set—the set of all possible system trajectories that arise from different initial conditions, uncontrolled inputs, and inherent switching. Verification was performed by checking that the reach set is contained within a region of the state-space defined by the system performance requirements. Algorithms to solve the reachability problem for power electronics systems operating under both open-loop and closed-loop control were provided.

One of the advantages of this technique is that it provides a computationally tractable solution to the large-signal behavior verification problem for power electronics systems. This method can substantially reduce the computational burden of existing time-domain simulation-based large-signal behavior verification methods, which rely on performing a large number of simulations in order to capture the behavior of the system for all possible operating conditions. Finally, although not pursued in this paper, the analytically tractable solutions provided by the proposed method also give further insight into the influence of design parameters and control techniques on the overall system performance.

References

[1] J. Kassakian, M. Schlecht, and G. Verghese, *Principles of Power Electronics*. Reading, MA: Addison-Wesley, 1991.

[2] P. Krein, *Elements of Power Electronics*. New York, NY: Oxford University Press, 1997.

[3] R. Erickson and D. Maksimović, *Fundamentals of Power Electronics*, 2nd ed. Norwell, MA: Kluwer Academic Publishers, 2001.

[4] N. Mohan, T. Undeland, and W. Robbins, *Power Electronics: Converters, Applications, and Design*, 3rd ed. Hoboken, NJ: Wiley, 2003.

[5] C. Chen, *Linear System Theory and Design*, 3rd ed. New York, NY: Oxford University Press, 1999.

[6] X. Zhou, P. Xu, and F. Lee, "A novel current-sharing control technique for low-voltage high-current voltage regulator module applications," *IEEE Transactions on Power Electronics*, vol. 15, no. 6, pp. 1153 – 1162, Nov. 2000.

[7] Z. Mihajlovic, B. Lehman, and C. Sun, "Output ripple analysis of switching DC-DC converters," *IEEE Transactions on Circuits and Systems I: Regular Papers*, vol. 51, no. 8, pp. 1596 – 1611, Aug. 2004.

[8] W. Huang, D. Clavette, G. Schuellein, M. Crowther, and J. Wallace, "System accuracy analysis of the multiphase voltage regulator module," *IEEE Transactions on Power Electronics*, vol. 22, no. 3, pp. 1019–1026, May 2007.

[9] Q. Li, F. Lee, and T. Wilson Jr., "Design verification and testing of power supply system by using virtual prototype," *IEEE Transactions on Power Electronics*, vol. 18, no. 3, pp. 733–739, May 2003.

[10] L. Kamas and S. Sanders, "Power electronic circuit reliability analysis incorporating parallel simulations," in *Proc. IEEE Workshop on Computers in Power Electronics*, Aug. 1996, pp. 45–51.

[11] M. del Casale, N. Femia, P. Lamberti, and V. Mainardi, "Selection of optimal closed-loop controllers for DC-DC voltage regulators based on nominal and tolerance design," *IEEE Transactions on Industrial Electronics*, vol. 51, no. 4, pp. 840–849, Aug. 2004.

[12] G. Garcera, E. Figueres, M. Pascual, and J. Benavent, "Robust model following control of parallel buck converters," *IEEE Transactions on Aerospace and Electronic Systems*, vol. 40, no. 3, pp. 983–997, July 2004.

[13] J. He, J. Jiang, J. Huang, and W. Chen, "Model of EMI coupling paths for an off-line power converter," in *Nineteenth Annual IEEE Applied Power Electronics Conference and Exposition, 2004*, vol. 2, 2004, pp. 708–713.

[14] S. Sanders, J. Noworolski, X. Liu, and G. Verghese, "Generalized averaging method for power conversion circuits," *IEEE Transactions on Power Electronics*, vol. 6, no. 2, pp. 251 –259, apr 1991.

[15] J. White and S. Leeb, "An envelope-following approach to switching power converter simulation," *IEEE Transactions on Power Electronics*, vol. 6, no. 2, pp. 303 –307, apr 1991.

[16] A. Domínguez-García and P. Krein, "Integrating reliability into the design of fault-tolerant power electronics systems," in *Proceedings of PESC 2008*, Rhodes, Greece, June 2008, pp. 2665–2671.

[17] E. M. Hope and A. D. Domínguez-García, "Design verification of power electronics systems subject to bounded uncertain inputs," in *IEEE Energy Conversion Congress and Exposition, 2009*, Sept. 2009, pp. 1126–1132.

[18] A. Chutinan and B. H. Krogh, "Computing polyhedral approximations to flow pipes for dynamic systems," in *Proceedings of the 37th IEEE Conference on Decision and Control*, vol. 2, Tampa, FL, Dec. 1998, pp. 2089–2094.

[19] A. Girard, "Reachability of uncertain linear systems using zonotopes," in *Proceedings of HSCC 2005*, Zurich, Switzerland, 2005, pp. 291–305.

[20] A. Chutinan and B. H. Krogh, "Computational techniques for hybrid system verification," *IEEE Transactions on Automatic Control*, vol. 48, no. 1, pp. 64–75, Jan. 2003.

[21] E. Asarin, T. Dang, G. Frehse, A. Girard, C. LeGuernic, and O. Maler, "Recent progress in continuous and hybrid reachability analysis," in *IEEE International Symposium on Computer-Aided Control Systems Design*, Munich, Germany, 2006, pp. 1582–1587.

[22] F. Schweppe, *Uncertain Dynamic Systems*. Englewood Cliffs, NJ: Prentice-Hall Inc., 1973.

[23] F. Chernousko, "Guaranteed estimation of reachable sets for controlled systems," in *Stochastic Optimization*. Berlin, Germany: Springer, 1986, pp. 619–631.

[24] A. Kurzhanski and P. Varaiya, "Ellipsoidal techniques for reachability analysis. Parts I & II," *Optimization Methods and Software*, vol. 17, pp. 177–206 and 207–237, Feb. 2000.

[25] ——, "On ellipsoidal techniques for reachability analysis. Part I: External approximations. Part II: Internal approximations, box-valued constraints," *Optimization Methods and Software*, vol. 17, no. 2, pp. 207–237, Jan. 2002.

[26] A. Kurzhanski, I. Mitchell, and P. Varaiya, "Ellipsoidal techniques for hybrid dynamics: The reachability problem," *Optimization Theory and Applications*, vol. 128, no. 3, pp. 499–521, March 2006.

[27] D. Liberzon, *Switching in Systems and Control*. Boston, MA: Birkhauser, 2003.

[28] H. Khalil, *Nonlinear Systems*. Upper Saddle River, NJ: Prentice-Hall, 2002.
[29] A. Kurzhanski and P. Varaiya. (2006) Ellipsoidal toolbox. [Online]. Available: http://www.eecs.berkeley.edu/akurzhan/ellipsoids/
[30] Plexim GmbH. (2009) Piece-wise linear electric circuit simulation. [Online]. Available: http://www.plexim.com
[31] J. Sun, "Characterization and performance comparison of ripple-based control for voltage regulator modules," *IEEE Transactions on Power Electronics*, vol. 21, no. 2, pp. 346 – 353, 2006.
[32] R. Redl and J. Sun, "Ripple-based control of switching regulators—an overview," *IEEE Transactions on Power Electronics*, vol. 24, no. 12, pp. 2669 –2680, 2009.
[33] J. Li and F. Lee, "Modeling of V^2 current-mode control," *IEEE Transactions on Circuits and Systems I: Regular Papers*, vol. 57, no. 9, pp. 2552 –2563, 2010.

Eric M. Hope received his B.S. and M.S. degrees in Electrical Engineering from the Illinois Institute of Technology in 2008, and the University of Illinois, Urbana-Champaign in 2009, respectively.

Xichen Jiang received his B.S. degree in Electrical Engineering from the University of Illinois, Urbana-Champaign in 2010 and is currently pursuing an M.S. degree. His research interests include control systems and power system reliability.

Alejandro D. Domínguez-García is an Assistant Professor in the Electrical and Computer Engineering Department at the University of Illinois, Urbana, where he is affiliated with the Power and Energy Systems area. His research interests are in the areas of system reliability theory and control, with a special focus on developing analytical and simulation tools to address the analysis, design and operation of electrical energy systems and components. He received the Ph.D. degree in Electrical Engineering and Computer Science from the Massachusetts Institute of Technology, Cambridge, MA, in 2007 and the degree of Electrical Engineer from the University of Oviedo (Spain) in 2001. After finishing his Ph.D., he spent some time as a post-doctoral research associate at the Laboratory for Electromagnetic and Electronic Systems of the Massachusetts Institute of Technology. Dr. Domnguez-Garca received the NSF CAREER Award in 2010.